

Translation Consistent Semi-supervised Segmentation for 3D Medical Images

Yuyuan Liu¹ Yu Tian¹ Chong Wang¹ Yuanhong Chen¹
Fengbei Liu¹ Vasileios Belagiannis² Gustavo Carneiro¹

¹ Australian Institute for Machine Learning, University of Adelaide

² Universität Ulm, Germany

Abstract. 3D medical image segmentation methods have been successful, but their dependence on large amounts of voxel-level annotated data is a disadvantage that needs to be addressed given the high cost to obtain such annotation. Semi-supervised learning (SSL) solve this issue by training models with a large unlabelled and a small labelled dataset. The most successful SSL approaches are based on consistency learning that minimises the distance between model responses obtained from perturbed views of the unlabelled data. These perturbations usually keep the spatial input context between views fairly consistent, which may cause the model to learn segmentation patterns from the spatial input contexts instead of the segmented objects. In this paper, we introduce the Translation Consistent Co-training (TraCoCo) which is a consistency learning SSL method that perturbs the input data views by varying their spatial input context, allowing the model to learn segmentation patterns from visual objects. Furthermore, we propose the replacement of the commonly used mean squared error (MSE) semi-supervised loss by a new Cross-model confident Binary Cross entropy (CBC) loss, which improves training convergence and keeps the robustness to co-training pseudo-labelling mistakes. We also extend CutMix augmentation to 3D SSL to further improve generalisation. Our TraCoCo shows state-of-the-art results for the Left Atrium (LA) and Brain Tumor Segmentation (BRaTS19) datasets with different backbones. Our code is available at <https://github.com/yyliau01/TraCoCo>.

Keywords: Medical Image Segmentation · Semi-supervised Learning · Translation Consistent · Semi-supervised Segmentation

1 Introduction

The training of 3D medical image segmentation neural network methods requires large sets of voxel-wise annotated samples. These sets are obtained using a laborious and expensive slice-by-slice annotation process, so alternative methods based on small labelled set training methods have been sought. One example is semi-supervised learning (SSL) that relies on a large unlabelled set and a small labelled set to train the model, and a particularly effective SSL approach is consistency learning that minimises the distance between the model responses obtained from different views of the unlabelled data [1, 2].

The different views of consistency learning methods can be obtained via data augmentation [3] or from the outputs of differently initialized networks [2, 4, 5]. Mean teacher (MT) [4, 6–9] combines these two perturbations and averages the

network parameters during training, yielding reliable pseudo-labels for the unlabelled data. However, the domain-specific transfer [3] of the teacher-student scheme can cause both networks to converge to a quite similar local minimum, reducing the network perturbation effectiveness. Recent approaches [2, 5] show that co-training provides an effective consistency regularization with the cross-supervision between two independent networks.

Even though successful, the approaches above can inadvertently learn the pattern from the spatial input context of the training data rather than from the visual objects to be segmented, which can yield unsatisfactory pseudo-labels for the unlabelled data. This issue is more pronounced in 3D medical data, where the smaller amount of training samples combined with the larger input data dimensionality can increase the dependence between the spatial input context and segmentation results, resulting in poor generalization. Hence, network perturbation combined with a perturbation of the spatial input context to form different views of unlabelled samples is an important technique to reduce the dependence between spatial input context and segmentation results. Such input context perturbation was exploited with the contrastive learning of intermediate features [10] for urban driving scenes’ segmentation. However, it depends on potentially mistaken segmentation predictions, which can lead to confirmation bias in the pixel-wise positive/negative sampling strategy, resulting in sub-optimal performance. Also, it does not explore network perturbations, which reduces its generalisation ability.

In this paper, we propose the Translation Consistent Co-training (TraCoCo). TraCoCo enforces the segmentation agreement inside the intersection region between translated views of the input data, where an additional log-likelihood regularization is applied to balance the importance of the segmented visual object and the background voxels. For the semi-supervised consistency loss, we propose the Cross-model confident Binary Cross-entropy (CBC) loss to replace the Mean Square Error (MSE), with the goal of improving training convergence while maintaining the robustness to pseudo-labelling mistakes. Moreover, CutMix [11] demonstrates significant improvements of the generalization in limited data situation [2], so we introduce CutMix for the 3D medical data to further improve the data diversity. In summary, we list our contributions below:

1. A novel co-training strategy based on translation consistency that is designed to promote cross-modal prediction consistency under spatial input context variation of the input data; (see Fig. 1);
2. A new entropy-based CBC loss that takes only the most confident pseudo labels to co-train the two models and improve training convergence compared with the commonly used MSE loss;
3. An extension of the 3D CutMix data augmentation to deal with the limited labelled data challenge in semi-supervised segmentation from 3D medical images.

Our approach yields state-of-the-art (SOTA) results for the semi-supervised benchmarks of the Left Atrium (LA) and Brain Tumor Segmentation 2019 (BRaTS19) datasets.

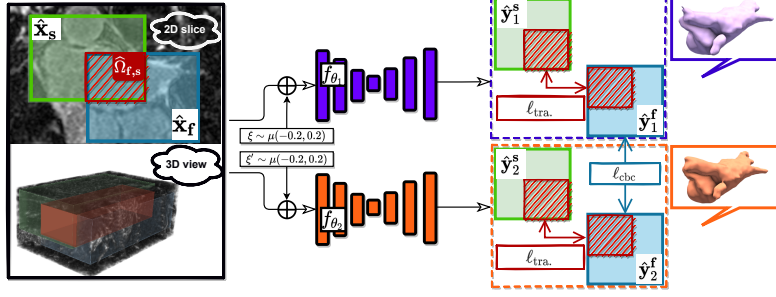


Fig. 1: **Learning with unlabelled data of TraCoCo.** The input volume \mathbf{x} is randomly cropped into sub-volumes $\hat{\mathbf{x}}_f$ in blue and the translated volume $\hat{\mathbf{x}}_s$ in green, where these sub-volumes have a non-empty intersection denoted by the lattice $\hat{\Omega}_{f,s} = \hat{\Omega}_f \cap \hat{\Omega}_s \neq \emptyset$, represented in red. This pair of sub-volumes are perturbed with uniform noise ξ before being used to produce the segmentation results $\{\hat{\mathbf{y}}_1^f, \hat{\mathbf{y}}_1^s\}, \{\hat{\mathbf{y}}_2^f, \hat{\mathbf{y}}_2^s\}$ from the networks f_{θ_1} and f_{θ_2} , respectively. The translation consistency loss $\ell_{\text{tra}}(\cdot)$ in (3) will penalise differences in the responses within $\hat{\Omega}_{f,s}$, and the outputs $\hat{\mathbf{y}}_1^f, \hat{\mathbf{y}}_2^f$ are used to minimize $\ell_{\text{cbc}}(\cdot)$ in (7). On the right-hand side, we show the 3D segmentations produced by the models (purple and orange volumes).

2 Method

For the 3D semi-supervised semantic segmentation, we have a small labelled set with $\mathcal{D}_L = \{(\mathbf{x}, \mathbf{y})_i\}_{i=1}^{|\mathcal{D}_L|}$, where $\mathbf{x} \in \mathcal{X} \subset \mathbb{R}^{H \times W \times C}$ represents the input volume with size $H \times W$ and C slices, and $\mathbf{y} \in \mathcal{Y} \subset \{0, 1\}^{H \times W \times C}$ denotes a binary (foreground vs background) segmentation ground truth. We also have a large unlabelled set $\mathcal{D}_U = \{\mathbf{x}_i\}_{i=1}^{|\mathcal{D}_U|}$, where $|\mathcal{D}_L| \ll |\mathcal{D}_U|$.

As depicted in Fig. 1, our approach is a co-training framework [12] that contains two differently initialised networks. Both segmentation models work with an input sub-volume $\hat{\mathcal{X}} \subset \mathbb{R}^{\hat{H} \times \hat{W} \times \hat{C}}$, where $\hat{H} < H$, $\hat{W} < W$, and $\hat{C} < C$. These sub-volumes are extracted from the original volume lattice Ω using the sub-lattice $\hat{\Omega}_f \subset \Omega$ of size $\hat{H} \times \hat{W} \times \hat{C}$ and centred at volume index $\mathbf{f} \in \mathbb{N}^3$. This sub-volume extracted from volume \mathbf{x} is represented by $\hat{\mathbf{x}}_f = \mathbf{x}(\hat{\Omega}_f)$. The models are represented by $f_{\theta} : \hat{\mathcal{X}} \rightarrow [0, 1]^{\hat{H} \times \hat{W} \times \hat{C}}$, where $\theta_1, \theta_2 \in \Theta \subset \mathbb{R}^P$ denote the P -dimensional parameters of the two models.

2.1 Translation Consistent Co-training (TraCoCo)

The proposed translation consistent co-training (TraCoCo) optimisation is based on the following loss function minimization:

$$\theta_1^*, \theta_2^* = \arg \min_{\theta_1, \theta_2} \ell_{\text{sup}}(\mathcal{D}_L, \theta_1, \theta_2) + \lambda \left(\ell_{\text{sem}}(\mathcal{D}_U, \theta_1, \theta_2) + \ell_{\text{tra}}(\mathcal{D}_L \cup \mathcal{D}_U, \theta_1, \theta_2) \right), \quad (1)$$

where the supervised learning loss

$$\ell_{sup}(\mathcal{D}_L, \theta_1, \theta_2) = \sum_{(\mathbf{x}, \mathbf{y}) \in \mathcal{D}_L} \ell_{ce}(\mathbf{y}^f, \hat{\mathbf{y}}_1^f) + \ell_{ce}(\mathbf{y}^f, \hat{\mathbf{y}}_2^f) + \ell_{dice}(\mathbf{y}^f, \hat{\mathbf{y}}_1^f) + \ell_{dice}(\mathbf{y}^f, \hat{\mathbf{y}}_2^f), \quad (2)$$

with $\ell_{ce}(\cdot)$ denoting the voxel-wise cross-entropy loss, $\ell_{dice}(\cdot)$ representing the volume-wise linearised Dice loss [6], $\hat{\mathbf{y}}_1^f = f_{\theta_1}(\hat{\mathbf{x}}_{\mathbf{f}} + \xi)$ (similarly for $\hat{\mathbf{y}}_2^f$, with $\xi \sim \mu(-0.2, 0.2)$ denoting a sample from a uniform distribution in the range $[-0.2, 0.2]$, and $\mathbf{y}^f = \mathbf{y}(\hat{\Omega}_{\mathbf{f}})$ representing the sub-volume label. Also in (1), $\ell_{sem}(\cdot)$, defined below in (6), represents the semi-supervised loss that uses the pseudo labels from the two models, $\ell_{tra}(\cdot)$, defined below in (3), denotes the translation consistency loss which enforces the cross-model consistency between the segmentation of two randomly-cropped sub-regions (containing varying spatial input contexts) of the original volume, and λ is a cosine ramp-up function that controls the trade-off between the losses.

Translation consistency loss. We take the training volume $\mathbf{x} \in \mathcal{D}_L \cup \mathcal{D}_U$, and extract two sub-volumes centred at $\mathbf{f}, \mathbf{s} \in \mathbb{N}^3$, with $\mathbf{f} \neq \mathbf{s}$ and denoted by $\hat{\mathbf{x}}_{\mathbf{f}}$ and $\hat{\mathbf{x}}_{\mathbf{s}}$ where their respective lattices have a non-empty intersection, i.e., $\hat{\Omega}_{\mathbf{f}, \mathbf{s}} = \hat{\Omega}_{\mathbf{f}} \cap \hat{\Omega}_{\mathbf{s}} \neq \emptyset$. Our proposed translation consistency loss from (1) is defined by

$$\ell_{tra}(\mathcal{D}_L \cup \mathcal{D}_U, \theta_1, \theta_2) = \sum_{\substack{\mathbf{x} \in \mathcal{D}_L \cup \mathcal{D}_U \\ \mathbf{f}, \mathbf{s} \sim \mathcal{U}(\Omega)}} \ell_{kl}(\mathbf{x}(\hat{\Omega}_{\mathbf{f}, \mathbf{s}}), \theta_1, \theta_2) + \alpha \ell_{reg}(\mathbf{x}(\hat{\Omega}_{\mathbf{f}, \mathbf{s}}), \theta_1, \theta_2), \quad (3)$$

where the centres of the two sub-volumes denoted by \mathbf{f}, \mathbf{s} are uniformly sampled from the original volume lattice Ω , α is a hyper-parameter to balance the two loss functions ($\alpha = 0.1$ for all the experiments),

$$\ell_{kl}(\mathbf{x}(\hat{\Omega}_{\mathbf{f}, \mathbf{s}}), \theta_1, \theta_2) = \sum_{\omega \in \hat{\Omega}_{\mathbf{f}, \mathbf{s}}} \mathbb{KL}(\hat{\mathbf{y}}_1^f(\omega), \hat{\mathbf{y}}_1^s(\omega)) + \mathbb{KL}(\hat{\mathbf{y}}_2^f(\omega), \hat{\mathbf{y}}_2^s(\omega)) \quad (4)$$

computes the Kullback-Leibler (KL) divergence between the segmentation outputs of the two models in the intersection region of two translated input sub-volumes represented by $\hat{\Omega}_{\mathbf{f}, \mathbf{s}}$, and $\hat{\mathbf{y}}_1^f, \hat{\mathbf{y}}_1^s, \hat{\mathbf{y}}_2^f$, and $\hat{\mathbf{y}}_2^s$ are defined in (2). Also in (3), we have

$$\ell_{reg}(\mathbf{x}(\hat{\Omega}_{\mathbf{f}, \mathbf{s}}), \theta_1, \theta_2) = - \sum_{\omega \in \hat{\Omega}_{\mathbf{f}, \mathbf{s}}} \mathbb{H}(\hat{\mathbf{y}}_1^f(\omega)) + \mathbb{H}(\hat{\mathbf{y}}_2^f(\omega)) + \mathbb{H}(\hat{\mathbf{y}}_1^s(\omega)) + \mathbb{H}(\hat{\mathbf{y}}_2^s(\omega)) \quad (5)$$

that aims to balance the foreground and background classes in the training voxels, where $\mathbb{H}(\cdot)$ represents Shannon’s entropy.

Semi-supervised cross-model confident binary cross-entropy (CBC) loss. The semi-supervised loss $\ell_{sem}(\cdot)$ in (1) enforces the consistency between the segmentation results by the two models, as follows:

$$\ell_{sem}(\mathcal{D}_U, \theta_1, \theta_2) = \sum_{\mathbf{x} \in \mathcal{D}_U} \ell_{cbc}(\hat{\mathbf{y}}_1^f, \hat{\mathbf{y}}_2^f) + \ell_{cbc}(\hat{\mathbf{y}}_2^f, \hat{\mathbf{y}}_1^f), \quad (6)$$

where

$$\ell_{cbc}(\hat{\mathbf{y}}_1^f, \hat{\mathbf{y}}_2^f) = -\sum_{\omega \in \hat{\Omega}_f} \mathbb{I}(\hat{\mathbf{y}}_1^f(\omega)[1] > \gamma) \log(\hat{\mathbf{y}}_2^f(\omega)[1]) + \mathbb{I}(\hat{\mathbf{y}}_1^f(\omega)[1] < \beta)(1 - \log(\hat{\mathbf{y}}_2^f(\omega)[1])), \quad (7)$$

with $\mathbb{I}(\cdot)$ denoting the indicator function, $\hat{\mathbf{y}}_1^f(\omega) \in [0, 1]^2$ representing the background ($\hat{\mathbf{y}}_1^f(\omega)[0]$) and foreground ($\hat{\mathbf{y}}_1^f(\omega)[1]$) segmentation probabilities in voxel $\omega \in \hat{\Omega}_f$ obtained from the softmax activation function, and γ, β representing hyper-parameters to balance the foreground and background losses. Note that our proposed $\ell_{cbc}(\cdot)$ replaces the more common MSE loss [6–8, 13–15] used in semi-supervised learning methods, where our goal is to maintain the MSE robustness to the pseudo-label mistakes and improve training convergence. In (7) we only allow the confidently classified foreground and background voxels by the first model to have their log probabilities maximised for the second model, and vice-versa ($\gamma = 0.65$ and $\beta = 0.1$ for all experiments).

3D CutMix. To improve training generalisation using the semi-supervised loss in (6), we extend CutMix [2, 16] to 3D data. This is achieved by defining a binary mask $\mathbf{m} \in \{0, 1\}^{H \times W \times C}$ to be applied to a pair of volumes with $\nu_{ij}^m = (1 - \mathbf{m}) \odot \mathbf{x}_i + \mathbf{m} \odot \mathbf{x}_j$, where the prediction from the model is obtained with $f_\theta(\nu_{ij}^m(\hat{\Omega}_f) + \xi)$. The pseudo labels from the second model is defined by $\hat{\mathbf{y}}_{2,ij}^f = (1 - \mathbf{m}) \odot \hat{\mathbf{y}}_{2,i}^f + \mathbf{m} \odot \hat{\mathbf{y}}_{2,j}^f$, with $\hat{\mathbf{y}}_{2,i}^f = f_{\theta_2}(\hat{\mathbf{x}}_i^f + \xi')$ and $\hat{\mathbf{y}}_{2,j}^f = f_{\theta_2}(\hat{\mathbf{x}}_j^f + \xi')$. To account for the 3D CutMix, the semi-supervised loss in (6) is re-defined with

$$\ell_{sem}(\mathcal{D}_U, \theta_1, \theta_2) = \sum_{\mathbf{x}_i, \mathbf{x}_j \in \mathcal{D}_U} \ell_{cbc}(f_{\theta_1}(\nu_{ij}^m(\hat{\Omega}_f) + \xi), \hat{\mathbf{y}}_{2,ij}^f) + \ell_{cbc}(f_{\theta_2}(\nu_{ij}^m(\hat{\Omega}_f) + \xi), \hat{\mathbf{y}}_{1,ij}^f). \quad (8)$$

3 Experiments and Results

Datasets. We validate our approach on two MRI datasets, namely Left Atrium (LA) and Brain Tumour Segmentation 2019 (BraTS19). LA is from the *Atrial Segmentation Challenge*¹ that contains 100 3D MRI volumes and their segmentation masks. Following previous papers [6, 13], we crop at the centre of the heart region in the pre-processing stage and use 80 volumes for training and 20 for testing (we use the same training and testing sample IDs as in [6, 13]). BRaTS19 is from the *Brain Tumor Segmentation Challenge*² and contains 335 brain MRIs with tumour segmentation labels. For pre-processing the volumes, we follow [17] and use only the FLAIR sequences which are cropped at the centre of the tumour region. We use 250 volumes for training, 25 for validation, and 60 for testing.

Implementation details. We use 3D-VNet [6] for the LA dataset, following [6, 13], and 3D-UNet [18] for the BRaTS19, following [17]. For both datasets, we set the initial learning rate to be $5e^{-2}$, and decay via the poly learning rate scheduler $(1 - \frac{\text{iter}}{\text{max_iter}})^{0.9}$. We set the number of iterations at 9,000 for LA and 30,000 for BRaTS. Component-based post-processing is commonly used in 3D organ segmentation [13, 19]. In this work, we adopt the connected components threshold (CCT) [20] as a post-processing to reject small isolated segmentation

¹ <http://atriaseg2018.cardiacatlas.org/>

² <https://www.med.upenn.edu/cbica/brats-2019/>

Table 1: **Evaluation on the LA dataset using VNet** based on the partition protocols of 8 and 16 labelled data. The † indicates the results based on CCT post-processing [13].

Left Atrium	# scan used		metrics			
	labelled	unlabelled	Dice(%)	Jaccard(%)	ASD(Voxel)	95HD(Voxel)
DAP [21]	8	72	81.89	71.23	3.80	15.81
LG-ER-MT [7]	8	72	85.54	75.12	3.77	13.29
DUWM [22]	8	72	85.91	75.75	3.31	12.67
MC-Net [15]	8	72	87.71	78.31	2.18	9.36
Ours	8	72	89.29	80.82	2.28	6.92
UA-MT† [6]	8	72	84.57	73.96	2.90	12.51
SASSNet† [13]	8	72	87.32	77.72	2.55	9.62
Ours†	8	72	89.31	80.83	2.09	6.83
MT [4]	16	64	88.23	79.29	2.73	10.64
Entropy Mini. [23]	16	64	88.45	79.51	3.72	14.14
DAP [21]	16	64	87.89	78.72	2.74	9.29
CCT [1]	16	64	88.83	80.06	2.49	8.44
LG-ER-MT [7]	16	72	89.62	81.31	2.06	7.16
DUWM [22]	8	72	89.65	81.35	2.03	7.04
MC-Net [15]	16	64	90.34	82.48	1.77	6.00
Ours	16	64	90.94	83.47	1.79	5.49
UA-MT† [6]	16	64	89.11	80.62	2.21	7.30
SASSNet† [13]	16	64	89.54	81.24	2.20	8.24
Ours†	16	64	90.96	83.49	1.70	5.45

regions, where the minimum volume size is set to be $(10 \times 10 \times 10)$ voxels. More details are shown in the Supplementary Material (Sec. 1 and Sec. 2).

Evaluation Measures. We use four measures to quantitatively evaluate our method, which are Dice, Jaccard, the average surface distance (ASD), and the 95% Hausdorff Distance (95HD). The Dice and Jaccard are measured in percentage, while ASD and 95HD are measured in voxels.

Comparison with SOTA approaches. Our experimental results improve the SOTA for both of the LA (shown in Tab. 1) and BRaTS19 (shown in Tab. 2) datasets. In the **LA dataset**, our method without post-processing ('Ours') yields better performance than the SOTA for all measures, except for ASD. This can be explained by our approach being less overfitted to spatial input contexts, but more sensitive to foreground noise. *Therefore, the results contain isolated small segmentation regions that are far from the main segmentation surface, leading to worse ASD but better 95HD.* The CCT post-processing ('Ours†') solves this issue, with small increase of 0.026 sec/volume of processing time. For the **BRaTS19 dataset**, we run the SOTA methods using the code from the published papers, but with small modifications to adapt them to our 3D-UNet backbone. Similarly to the LA dataset, Tab. 2 shows that our approach ('Ours') outperforms previous SOTA methods using the overlap measures. For example, our approach increases Dice by 1.09% and 1.02%, compared with SASSNet [13] and LG-ER-MT [7] under the 50-sample partition protocol. Furthermore, our method with post-processing shows the best results for all measures.

Improvement over supervised baselines. We compare our results with fully supervised learning (trained with the same labelled set indicated by the partition protocol) using 3D-VNet on LA in Fig. 2a and 3D-UNet on BRaTS19 in Fig. 2b. The two figures demonstrate that our approach successfully leverages

Table 2: **Evaluation on the BRaTS19 dataset using UNet** based on different partition protocols of 25 and 50 labeled data. The † indicates the results based on CCT post-processing [13].

BRaTS2019	# scan used		metrics			
	labelled	unlabelled	Dice(%)	Jaccard(%)	ASD(Voxel)	95HD(Voxel)
UA-MT [6]	25	225	84.64	74.76	2.36	10.47
Entropy Mini. [23]	25	225	84.55	74.58	2.18	9.62
ICT [24]	25	225	83.71	73.62	2.65	12.09
SASSNet [13]	25	225	84.73	74.89	2.44	9.88
LG-ER-MT [7]	25	225	84.75	74.97	2.21	9.56
Ours	25	225	85.71	76.39	2.27	9.20
LG-ER-MT [7]†	25	225	84.82	75.03	2.16	8.96
Ours†	25	225	85.79	76.45	2.11	8.43
UA-MT [6]	50	200	85.32	75.93	1.98	8.68
Entropy Mini. [23]	50	200	85.61	76.27	1.91	8.57
ICT [24]	50	200	84.85	75.34	2.13	9.13
SASSNet [13]	50	200	85.64	76.33	2.04	9.17
LG-ER-MT [7]	50	250	85.67	76.36	1.99	8.92
Ours	50	200	86.69	77.69	1.93	8.04
LG-ER-MT [7]†	50	250	85.70	76.52	1.89	8.23
Ours†	50	200	86.73	77.75	1.75	7.69

unlabelled data and brings a dramatic performance boost. Particularly in the few-labelled data setup, our approach brings 8.26% Dice improvement for 8 labelled samples on LA and 4.1% for 25 labelled samples on BRaTS19. Our approach yields consistent improvements for more labelled data, such as 3.59% and 2.41% for 16 and 32 volumes, respectively, on LA, and 2.85% and 1.49% for 50 and 125 volumes, respectively, on BRaTS19.

Ablation study. We first present the ablation studies of the different components of our approach on the LA dataset in Tab. 3a. We use the co-training [12] with MSE loss as baseline Co-T. Replacing the MSE loss by our CBC loss brings a 1.02% Dice improvement. The translation consistency training further increases Dice by 0.89%. Moreover, the proposed 3D CutMix improves Dice by 0.21%. In Tab. 3b, we study different types of losses to be used by the semi-supervised loss $\ell_{sem}(\cdot)$ in (6) on LA dataset. If we replace the CBC loss by the widely used MSE loss, we see a drop of almost 1.2% Dice. The KL divergence loss shows a 0.9% worse Dice, while the CE and BCA losses, which disregard pseudo-label confidence, decrease Dice by around 0.5%.

Visualization Results. Fig. 3 shows the SASSNet [13], UA-MT [6], fully supervised and our results for LA and BRaTS19 images, with 16 and 25 labelled data protocols. We argue that the results from our method is visually closer to the ground truth than competing approaches.

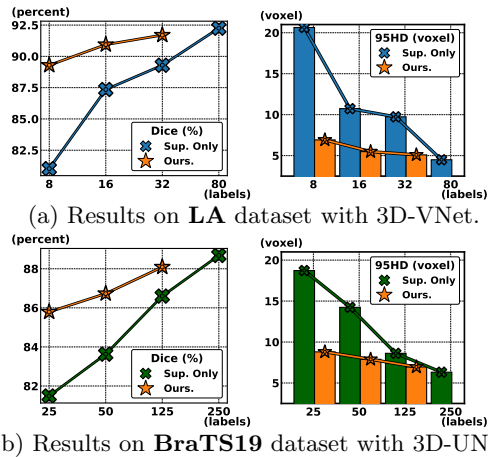


Fig. 2: **Improvements over the supervised baseline** upon different partition protocols.

Table 3: **Ablation studies on LA dataset:** (a) shows the ablation study, and (b) presents the ℓ_{sem} ablation assuming *all components are present in the model*. Co-T denotes co-training with MSE loss, CBC is our proposed semi-supervised loss, TraCo is translation consistency, and CM represents 3D-CutMix. MSE, KL, CE, BCE are different types of semi-supervised losses.

(a) The **components** ablation studies. (b) Semi-supervised **loss** study.

Co-T	CBC	TraCo	CM	Dice	95HD	ℓ_{sup}	ℓ_{sem}					Dice	95HD
							MSE	KL	CE	BCE	CBC		
✓				88.82	7.416	✓	✓					89.77	6.798
✓	✓			89.84	6.455	✓		✓				90.01	7.832
✓	✓	✓		90.73	6.145	✓			✓			90.50	6.744
✓	✓			90.42	7.130	✓			✓			90.42	7.130
✓	✓	✓	✓	90.94	5.489	✓				✓		90.94	5.489

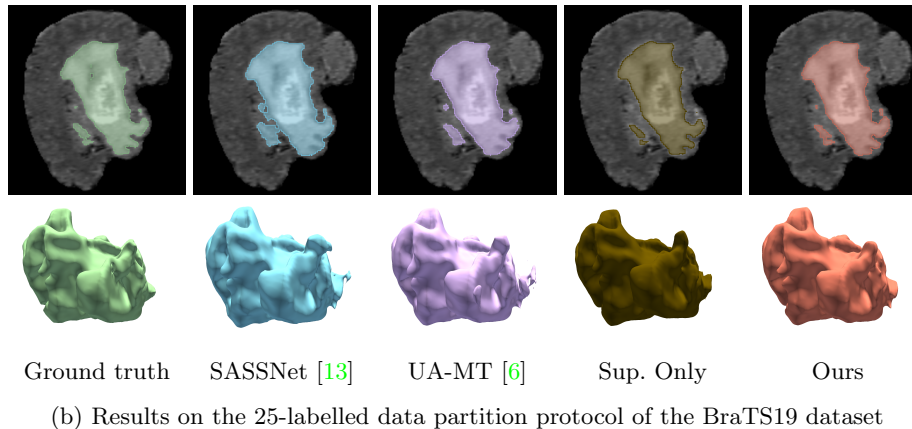
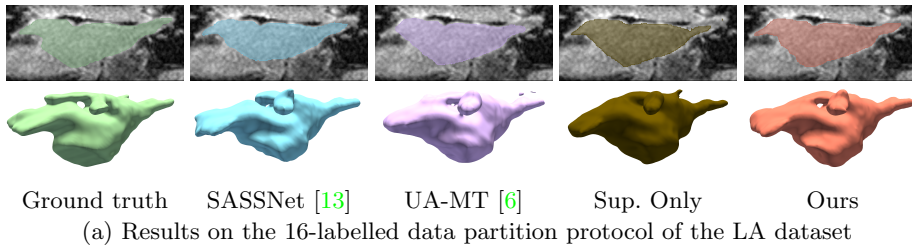


Fig. 3: **Qualitative segmentation results.**

4 Conclusions

In this paper, we presented TraCoCo, which is a new type of perturbation that varies the input data spatial context to reduce the dependencies between segmented objects and background patterns. Moreover, our proposed entropy-based CBC loss trains one model based on the other model’s confident predictions, yielding a better convergence than other SSL losses. The comparison with the SOTA shows that our approach produces the most accurate segmentation results both on LA and BRaTS19. In order to deal with the efficiency challenges for large volumes in practice, more attention will be drawn to decreasing the FP rate without the usage of post-processing in the future.

References

1. Yassine Ouali, Céline Hudelot, and Myriam Tami. Semi-supervised semantic segmentation with cross-consistency training. In *Proceedings of the IEEE/CVF Conference on Computer Vision and Pattern Recognition*, pages 12674–12684, 2020. [1](#), [6](#)
2. Xiaokang Chen, Yuhui Yuan, Gang Zeng, and Jingdong Wang. Semi-supervised semantic segmentation with cross pseudo supervision. In *IEEE Conference on Computer Vision and Pattern Recognition (CVPR)*, 2021. [1](#), [2](#), [5](#)
3. David Berthelot, Nicholas Carlini, Ian Goodfellow, Nicolas Papernot, Avital Oliver, and Colin Raffel. Mixmatch: A holistic approach to semi-supervised learning. *arXiv preprint arXiv:1905.02249*, 2019. [1](#), [2](#)
4. Antti Tarvainen and Harri Valpola. Mean teachers are better role models: Weight-averaged consistency targets improve semi-supervised deep learning results. *arXiv preprint arXiv:1703.01780*, 2017. [1](#), [6](#)
5. Zhanghan Ke, Di Qiu, Kaican Li, Qiong Yan, and Rynson WH Lau. Guided collaborative training for pixel-wise semi-supervised learning. In *Computer Vision—ECCV 2020: 16th European Conference, Glasgow, UK, August 23–28, 2020, Proceedings, Part XIII 16*, pages 429–445. Springer, 2020. [1](#), [2](#)
6. Lequan Yu, Shujun Wang, Xiaomeng Li, Chi-Wing Fu, and Pheng-Ann Heng. Uncertainty-aware self-ensembling model for semi-supervised 3d left atrium segmentation. In *International Conference on Medical Image Computing and Computer-Assisted Intervention*, pages 605–613. Springer, 2019. [1](#), [4](#), [5](#), [6](#), [7](#), [8](#), [11](#)
7. Wenlong Hang, Wei Feng, Shuang Liang, Lequan Yu, Qiong Wang, Kup-Sze Choi, and Jing Qin. Local and global structure-aware entropy regularized mean teacher model for 3d left atrium segmentation. In *International Conference on Medical Image Computing and Computer-Assisted Intervention*, pages 562–571. Springer, 2020. [1](#), [5](#), [6](#), [7](#)
8. Kaiping Wang, Bo Zhan, Chen Zu, Xi Wu, Jiliu Zhou, Luping Zhou, and Yan Wang. Triple-uncertainty guided mean teacher model for semi-supervised medical image segmentation. In *International Conference on Medical Image Computing and Computer-Assisted Intervention*, pages 450–460. Springer, 2021. [1](#), [5](#)
9. Yuyuan Liu, Yu Tian, Yuanhong Chen, Fengbei Liu, Vasileios Belagiannis, and Gustavo Carneiro. Perturbed and strict mean teachers for semi-supervised semantic segmentation. *arXiv preprint arXiv:2111.12903*, 2021. [1](#)
10. Xin Lai, Zhuotao Tian, Li Jiang, Shu Liu, Hengshuang Zhao, Liwei Wang, and Jiaya Jia. Semi-supervised semantic segmentation with directional context-aware consistency. In *Proceedings of the IEEE/CVF Conference on Computer Vision and Pattern Recognition*, pages 1205–1214, 2021. [2](#)
11. Sangdoon Yun, Dongyoon Han, Seong Joon Oh, Sanghyuk Chun, Junsuk Choe, and Youngjoon Yoo. Cutmix: Regularization strategy to train strong classifiers with localizable features. In *Proceedings of the IEEE/CVF International Conference on Computer Vision*, pages 6023–6032, 2019. [2](#)
12. Siyuan Qiao, Wei Shen, Zhishuai Zhang, Bo Wang, and Alan Yuille. Deep co-training for semi-supervised image recognition. In *Proceedings of the european conference on computer vision (eccv)*, pages 135–152, 2018. [3](#), [7](#)
13. Shuailin Li, Chuyu Zhang, and Xuming He. Shape-aware semi-supervised 3d semantic segmentation for medical images. In *International Conference on Medical Image Computing and Computer-Assisted Intervention*, pages 552–561. Springer, 2020. [5](#), [6](#), [7](#), [8](#), [11](#), [12](#)

14. Shumeng Li, Ziyuan Zhao, Kaixin Xu, Zeng Zeng, and Cuntai Guan. Hierarchical consistency regularized mean teacher for semi-supervised 3d left atrium segmentation. *arXiv preprint arXiv:2105.10369*, 2021. [5](#)
15. Yicheng Wu, Minfeng Xu, Zongyuan Ge, Jianfei Cai, and Lei Zhang. Semi-supervised left atrium segmentation with mutual consistency training. *arXiv preprint arXiv:2103.02911*, 2021. [5](#), [6](#)
16. Geoff French, Samuli Laine, Timo Aila, Michal Mackiewicz, and Graham Finlayson. Semi-supervised semantic segmentation needs strong, varied perturbations. *arXiv preprint arXiv:1906.01916*, 2019. [5](#)
17. Shuai Chen, Gerda Bortsova, Antonio García-Uceda Juárez, Gijs van Tulder, and Marleen de Bruijne. Multi-task attention-based semi-supervised learning for medical image segmentation. In *International Conference on Medical Image Computing and Computer-Assisted Intervention*, pages 457–465. Springer, 2019. [5](#)
18. Özgün Çiçek, Ahmed Abdulkadir, Soeren S Lienkamp, Thomas Brox, and Olaf Ronneberger. 3d u-net: learning dense volumetric segmentation from sparse annotation. In *International conference on medical image computing and computer-assisted intervention*, pages 424–432. Springer, 2016. [5](#)
19. Fabian Isensee, Paul F Jaeger, Simon AA Kohl, Jens Petersen, and Klaus H Maier-Hein. nnu-net: a self-configuring method for deep learning-based biomedical image segmentation. *Nature methods*, 18(2):203–211, 2021. [5](#), [11](#)
20. Anita Khanna, Narendra D Londhe, S Gupta, and Ashish Semwal. A deep residual u-net convolutional neural network for automated lung segmentation in computed tomography images. *Biocybernetics and Biomedical Engineering*, 40(3):1314–1327, 2020. [5](#), [11](#)
21. Han Zheng, Lanfen Lin, Hongjie Hu, Qiaowei Zhang, Qingqing Chen, Yutaro Iwamoto, Xianhua Han, Yen-Wei Chen, Ruofeng Tong, and Jian Wu. Semi-supervised segmentation of liver using adversarial learning with deep atlas prior. In *International Conference on Medical Image Computing and Computer-Assisted Intervention*, pages 148–156. Springer, 2019. [6](#)
22. Yixin Wang, Yao Zhang, Jiang Tian, Cheng Zhong, Zhongchao Shi, Yang Zhang, and Zhiqiang He. Double-uncertainty weighted method for semi-supervised learning. In *International Conference on Medical Image Computing and Computer-Assisted Intervention*, pages 542–551. Springer, 2020. [6](#)
23. Tuan-Hung Vu, Himalaya Jain, Maxime Bucher, Matthieu Cord, and Patrick Pérez. Advent: Adversarial entropy minimization for domain adaptation in semantic segmentation. In *Proceedings of the IEEE/CVF Conference on Computer Vision and Pattern Recognition*, pages 2517–2526, 2019. [6](#), [7](#)
24. Vikas Verma, Kenji Kawaguchi, Alex Lamb, Juho Kannala, Yoshua Bengio, and David Lopez-Paz. Interpolation consistency training for semi-supervised learning. *arXiv preprint arXiv:1903.03825*, 2019. [7](#)
25. Wenshuai Zhao and Zengfeng Zeng. Multi scale supervised 3d u-net for kidney and tumor segmentation. *arXiv preprint arXiv:1908.03204*, 2019. [11](#)

Table 4: The comparison of the post-processing in **LA** dataset. NMS is the non-max suppression and CCT is the connected component threshold.

# label	Post-processing	Dice	Jaccard	ASD	95HD
8	w/o	89.29	80.82	2.28	6.92
	CCT	89.31	80.83	2.09	6.83
	NMS	89.28	80.80	1.95	7.35
16	w/o	90.94	83.47	1.79	5.49
	CCT	90.96	83.49	1.70	5.45
	NMS	90.93	83.45	1.62	5.90
32	w/o	91.70	84.75	1.69	5.09
	CCT	91.73	84.78	1.58	5.09
	NMS	91.69	84.73	1.51	5.55

A Implementation details

We use PyTorch to implement our code. In both architectures of UNet and VNet, we adopt mini-batch SGD with momentum to train our model, where the momentum is fixed at 0.9, and weight decay is set to 0.0005. To balance the supervised and unsupervised losses in training, we utilize *Cosine ramp-up* function with 40 iterations, starting with $\lambda = 0$.

Experiment Settings. In training, each batch consists of 2 voxel-wise labelled and 2 unlabelled volumes, and they are cropped to be of size $112 \times 112 \times 80$ on LA, and $96 \times 96 \times 96$ on BraTS19. We employ the same online augmentation with random crop and flipping, following [6, 13]. The semi-supervised learning experimental setup partitions the original training set for the LA dataset to have 8, 16 and 32 labelled samples and the remaining unlabelled. For the BRaTS19 dataset, the original training set is split to have 25, 50 and 125 labelled samples and the rest of samples remain unlabelled. During testing, we only use one network (i.e., $f_{\theta_1}(\cdot)$) to produce our results, where the final segmentation is obtained via the sliding window strategy.

Hardware Requirements. We use one **NVIDIA GeForce RTX 3090** GPU to implement our algorithm in LA dataset, and one 32GB **V100** for BRaTS19 because of the larger volume of input.

B Connected Component-based Post-processing

Connected Component-based post-processing is popular in medical image segmentation [19, 20, 25], and the isolated false positive (FP) outlier predictions is eliminated with non-max suppression (NMS) [13, 19] or a connected components threshold (CCT) [20]. In our work, we filter out the noisy regions that are smaller than approximately $\frac{1}{1500}$ of the entire input volume to reduce isolate FP regions. As shown in Tab. 4, CCT yields the best results for the Dice and IoU measurements with the filtering out of small isolated regions. The NMS slightly decreases the overlap measurements because it eliminates all isolated regions, even the ones that are potentially correct. Despite its success in ASD measurements, in practice, the foreground regions can be non-contiguous, but NMS will

eliminate all but the largest region. We believe those potential false negative (FN) regions are harmful, so we choose CCT as our post-processing strategy.

Inference Run-time. We evaluate the run-time of w/ and w/o CCT post-processing based on *cc3d*³ python package, following SASSNet [13]. For images in the LA dataset, our method runs in **1.386** (sec/volume) on average and **1.412** (sec/volume) with the CCT. Similarly, our method runs in **0.4268** (w/o CCT) and **0.4495** (w/ CCT) respectively, in Brats19 dataset.

³ <https://github.com/seung-lab/connected-components-3d>